Available online at www.sciencedirect.com
SCIENCE DIRECT®
Polymer 45 (2004) 893–903
polymer
www.elsevier.com/locate/polymer

Adhesion of polyethylene blends to polypropylene

B.C. Poon[a], S.P. Chum[b], A. Hiltner[a,*], E. Baer[a]

[a]*Department of Macromolecular Science and Engineering, and Center for Applied Polymer Research, Case Western Reserve University, 2100 Adelbert Road, Cleveland, OH 44106-7202, USA*
[b]*Polyolefins and Elastomers R&D, The Dow Chemical Company, Freeport, TX 77541, USA*

Received 3 September 2003; received in revised form 9 November 2003; accepted 14 November 2003

Abstract

The effect of chain microstructure on adhesion of ethylene copolymers to polypropylene (PP) was studied using coextruded microlayers. Adhesion was measured by delamination toughness G using the T-peel test, and interfacial morphology was examined by atomic force microscopy. Good adhesion to PP was achieved with homogeneous metallocene catalyzed copolymers (mPE) with density 0.90 g cm^{-3} or less. Good adhesion was attributed to entanglement bridges. In contrast, a heterogeneous Ziegler-Natta catalyzed copolymer (ZNPE) of density 0.925 g cm^{-3} exhibited poor adhesion to PP due to an amorphous interfacial layer of low molecular weight, highly branched fractions that prevented effective interaction of ZNPE bulk chains with PP. Blending mPE with ZNPE eliminated the amorphous interfacial layer and resulted in epitaxial crystallization of ZNPE bulk chains with some increase in G. Increasing the mPE content of the blend past the amount required to completely resolve the amorphous interfacial layer of ZNPE resulted in a steady, almost linear, increase in G. Phase separation of mPE and ZNPE during crystallization produced an interface with regions of epitaxially crystallized ZNPE bulk chains and other regions of entangled mPE chains. Entanglement bridges imparted much better adhesion than did epitaxially crystallized lamellae.

Keywords: Polyethylene; Polypropylene; Blends

1. Introduction

Blending polypropylene and ethylene copolymers to synergistically combine the properties of these two low-cost polymer families is an attractive option for a variety of applications in films and engineering thermoplastics [1]. Recent developments in catalyst technology have dramatically enhanced control over chain microstructure of polyolefins in production [2]. Synthesis of ethylene copolymers by metallocene catalysts introduced copolymers with homogeneous comonomer distribution and extended the practical range in comonomer content to low crystallinity elastomers. New catalyst systems are similarly extending the range for chain microstructures achievable in propylene homopolymers [3] and copolymers [4]. Exciting possibilities exist for combining these new polymers. However, as in any situation that brings two polymers into intimate contact, whether as polymer blends, alloys, or multilayer films, achieving synergistic property combinations depends on adhesion of the constituents.

Interfacial properties are not easily examined in the dispersed domain morphology of conventional melt blends. Microlayer coextrusion of many alternating layers of two polymers with individual layer thicknesses on the micron size scale creates a one-dimensional model of the melt blend [5,6]. Adhesion of two polymers in microlayers is conveniently studied with the T-peel test [7]. Although peel tests generally do not supply absolute adhesive energies, the delamination toughness obtained from the test provides useful comparisons if the testing parameters and specimen dimensions are kept constant [8].

Using coextruded microlayers of a heterogeneous Ziegler-Natta catalyzed ethylene copolymer (ZNPE) and isotactic polypropylene (PP), a previous study demonstrated that relatively poor adhesion of ZNPE to PP was due to the presence of an amorphous interfacial layer ~8 nm thick made up of low molecular weight, highly branched fractions of heterogeneous ZNPE [9]. A homogeneous metallocene catalyzed copolymer (mPE) with about the same short chain branch (SCB) content and about the same average molecular

* Corresponding author. Tel.: +1-2163684186; fax: +1-2163686329.
E-mail address: pah6@po.cwru.edu (A. Hiltner).

0032-3861/$ - see front matter © 2003 Elsevier Ltd. All rights reserved.
doi:10.1016/j.polymer.2003.11.018

weight as bulk chains of ZNPE did not possess a population of chains with composition different from the bulk that could segregate to the interface. Access of average chains to the interface resulted in epitaxial crystallization of mPE on the PP layer. As a consequence, the delamination toughness G was higher, 430 J m^{-2} for mPE compared to 140 J m^{-2} for ZNPE. Blending ZNPE with as little as 5% of a homogeneous copolymer having higher SCB content eliminated the interfacial layer by enhancing the miscibility of highly branched fractions and thereby increased G by allowing bulk ZNPE chains to epitaxially crystallize.

In this study, we consider adhesion of PP to blends of ZNPE with a homogeneous ethylene copolymer across the entire blend composition range. Adhesion to PP is measured as delamination toughness of microlayers, and correlations are made with interfacial structure as determined with atomic force microscopy. The effects of short chain branch content and molecular weight of the homogeneous ethylene copolymer are examined.

2. Experimental

The polymers used in the study are described in Table 1. The isotactic PP was PROFAX™ 6723 from Basell, the ZNPE was DOWLEX™ 2083 from Dow, and the polystyrene (PS) was STYRON™ 665 from Dow. Four experimental metallocene-catalyzed ethylene–octene copolymers (mPE) that differed in comonomer content and molecular weight were provided by The Dow Chemical Company. The melt flow index was measured at 190 °C with a load of 2.16 kg (I_2). Temperature rising elution fractionation (TREF) curves of the ethylene copolymers in Fig. 1 compare the SCB distribution of heterogeneous ZNPE and homogeneous mPE92, mPE90H, mPE90L, and mPE89.

Blends with compositions 100/0, 95/5, 90/10, 85/15, 75/25, 63/37, 50/50, 25/75, and 0/100 (ZNPE/mPE, wt/wt) were prepared in a Haake twin screw extruder with barrel temperature set at 200 °C. Blends were pelletized and coextruded as microlayers with PP in a 50/50 volume ratio. Tapes 12 mm wide and 1.6 mm thick with 33 alternating layers of PP and either ZNPE, mPE or a blend were coextruded into cold water. The layer thickness was approximately 50 μm. Microlayers of ZNPE, mPE and their blends with PS were coextruded under similar conditions.

Delamination was carried out with a modified T-peel test (ASTM D1876) [7]. Strips 6.4 mm wide and 8 cm long were cut from the center of the tape and notched by pushing a fresh razor blade into the midplane of the tape. The notch was examined with an optical microscope to ensure that the crack started along a single interface. Specimens were peeled at ambient temperature at various rates in an Instron Model 1122. At least two specimens of each composition were tested.

Microlayers were microtomed at −45 °C through the thickness of the tape and normal to the extrusion direction to expose a cross-section of the layer interface. The microtomed surface was etched for 30 min using a 2:1 (v/v) solution of sulfuric acid/orthophosphoric acid with 0.7 wt% potassium permanganate [10]. The etched surface was imaged in a Digital Instruments Nanoscope IIIa atomic force microscope (AFM) using medium tapping with a setpoint ratio (A/A_o) of 0.7–0.8 and a free oscillating tip amplitude (A_o) of 36 nm. Height and phase images were recorded simultaneously.

Attempts to cryogenically separate the layers, in order to observe the layer surfaces, resulted in damage to the surfaces even for compositions with the poorest adhesion. The layer surfaces of ZNPE, mPE90H and their blends in PP microlayers were mimicked by microlayering with PS under identical process conditions. The layers of the PS microlayers separated easily at liquid nitrogen temperature without damage to the surfaces. The surfaces were imaged by AFM in the tapping mode with A/A_o of 0.83 and A_o of 36 nm. Sometimes the ZNPE surface was washed with ethanol before imaging to remove amorphous low molecular weight ZNPE fractions.

3. Results and discussion

3.1. Delamination toughness

A series of T-peel curves for PP microlayered with ZNPE, mPE89 and their blends is shown in Fig. 2. The peel

Table 1
Materials

Material	Designation	Octene content[a] (mol%)	Density (kg m^{-3})	I_2[a] (g (10 min)$^{-1}$)	M_w[a] (kg mol^{-1})	M_w/M_n[a]
Isotactic polypropylene PROFAX™ 6723	PP			0.8		
Polystyrene STYRON™ 665	PS			1.0		
Ziegler-Natta polyethylene DOWLEX™ 2083	ZNPE	2.4	925	2.0	98	3.5
Metallocene polyethylene	mPE92	2.8	916	1.0	125	2.0
Metallocene polyethylene	mPE90H	4.7	902	1.2	144	2.1
Metallocene polyethylene	mPE90L	4.7	902	1.8	119	2.1
Metallocene polyethylene	mPE89	7.4	890	1.5	133	2.1

[a] Data for ethylene copolymers supplied by The Dow Chemical Company.

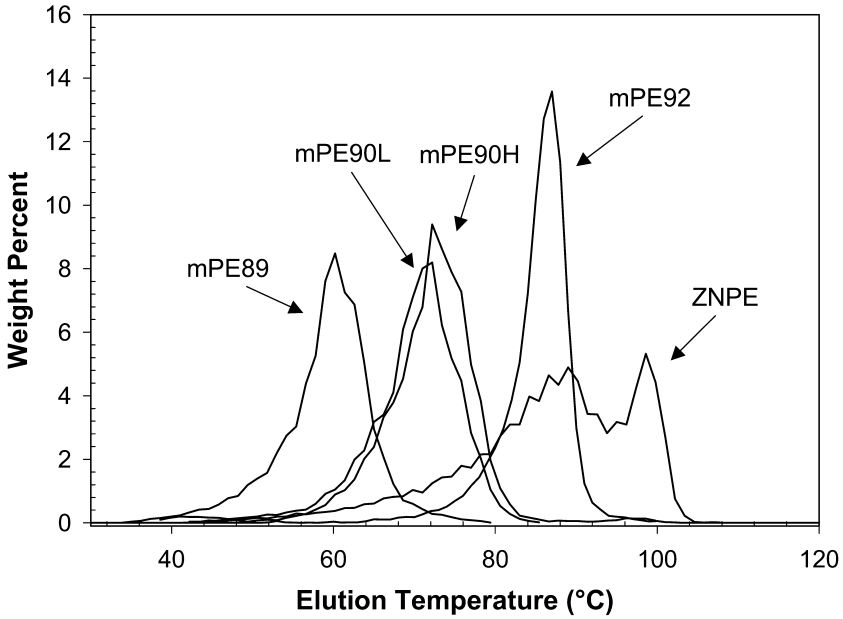

Fig. 1. TREF curves for ethylene copolymers. Data provided by The Dow Chemical Company.

curves were taken from the steady-state region, where the crack propagated at constant force after the beam arms reached the T-peel configuration. Constant peel force allowed calculation of the delamination toughness G using the relationship $G = 2F/w$, where F is the average peel force in the steady state region and w is the width of the specimen. In all cases, the crack propagated along the interface between a PP layer and a ZNPE layer as indicated by ATR-FTIR analysis of matching peel surfaces. This method probed to a depth of approximately one micron and showed only characteristic bands of ethylene copolymer on one surface and only characteristic bands of PP on the matching surface, even for microlayers that exhibited the highest G values. Addition of mPE89 to ZNPE steadily increased G from the low value of 140 J m^{-2} for ZNPE to the high value of 6800 J m^{-2} for mPE89. Most of the peel curves exhibited continuous crack propagation, however, intermediate blend compositions between 10 and 37% mPE89 exhibited stepwise crack propagation as indicated by the sawtooth pattern in the steady state region of the peel curve.

The change in crack propagation from continuous to stepwise to again continuous with increasing mPE89 content reflected how energy was dissipated during the peel process. For compositions with low mPE89 content, which exhibited poor adhesion, all the elastic energy stored

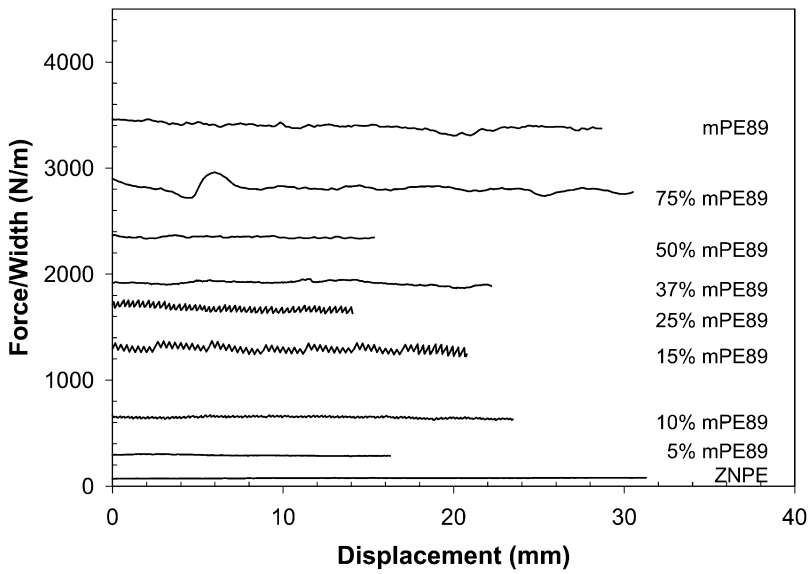

Fig. 2. Steady-state region of the peel curve, where the crack propagated at constant force after the beam arms reached the T-peel configuration. Delamination toughness G was calculated from the constant peel force.

in the beam arms was dissipated by crack propagation. As a result, crack growth was continuous. For compositions with higher mPE89 content, which exhibited better adhesion to PP, the elastic energy required to initiate the crack exceeded the energy required for crack propagation. When this occurred, the crack jumped and grew in an unstable manner until the stored energy was released [11]. Once the stored energy was released the crack stopped and remained stationary until the stored energy again increased enough to initiate the next crack jump. For compositions with high mPE89 content, which had very good adhesion to PP, the crack could not propagate fast enough to release stored elastic energy in the beam arms. As a result, the crack propagated continuously and the excess energy was dissipated through plastic beam arm deformation, as was evident from the curled beam arms.

Very good adhesion of mPE89 to PP raised concerns regarding the contribution of plastic deformation to the measured peel force. Indeed, examination of peeled specimens with high G values revealed permanent deformation of the beam arms. Visual inspection of the specimen from the side during the peel experiment confirmed stretching of the layers before final separation at the interface left featureless fracture surfaces. Reducing the peel rate can reduce plastic deformation to the extent that a rate-independent G is sometimes obtained [12]. Fig. 3 shows the reduction in G of the mPE copolymers as the peel rate was lowered. Essentially the same G values were obtained with mPE89 and mPE90H, somewhat lower G values with mPE90L, and the lowest G values with mPE92. However, the data did not demonstrate that a rate-independent G was achieved, even with a peel rate as low as 0.025 mm min^{-1}. Therefore, all subsequent peel data were obtained at 1 mm min^{-1}.

The effect of SCB content of the mPE constituent was examined using mPE89 and mPE90H, which had about the same molecular weight but different SCB. Although mPE89 and mPE90H exhibited the same delamination toughness to PP with G values over 6500 J m^{-2}, their blends with ZNPE did not exhibit the same compositional dependence of G, Fig. 4a. Blending even 5% of the higher SCB content mPE89 with ZNPE increased G from 140 to 580 J m^{-2}. The increase in G continued linearly to 3200 J m^{-2} for the blend with 25% mPE89, and continued albeit more gradually to 6600 J m^{-2} for mPE89. In contrast, 5% of the lower SCB content mPE90H had a very small effect, increasing G to only 200 J m^{-2}. Even 25% mPE90H increased G from 140 to only 630 J m^{-2}. However, more than 25% mPE90H increased G rapidly and linearly to a value of 6800 J m^{-2} for mPE90H.

The effect of molecular weight of the mPE constituent on G is shown in Fig. 4b with blends of mPE90H and mPE90L, which had the same SCB content but differed in molecular weight. In blends with 25% or less of the mPE constituent, molecular weight of mPE had almost no effect on G. Blending ZNPE with 25% of either mPE90H or mPE90L produced the same relatively small increase in G from 140 to about 600 J m^{-2}. This contrasted to the strong effect of SCB in this blend composition range (Fig. 4a). However, as the mPE content increased from 25 to 100%, G increased rapidly and linearly to 6800 J m^{-2} for mPE90H and 4900 J m^{-2} for mPE90L. Blends with mPE90H exhibited higher G than those containing the same amount of mPE90L. The difference reflected intrinsically higher G of mPE90H compared to mPE90L.

3.2. Amorphous interfacial layer

Poor adhesion of heterogeneous ZNPE to PP arose from segregation of low molecular weight, highly branched fractions at the interface. It is well-known that linear low

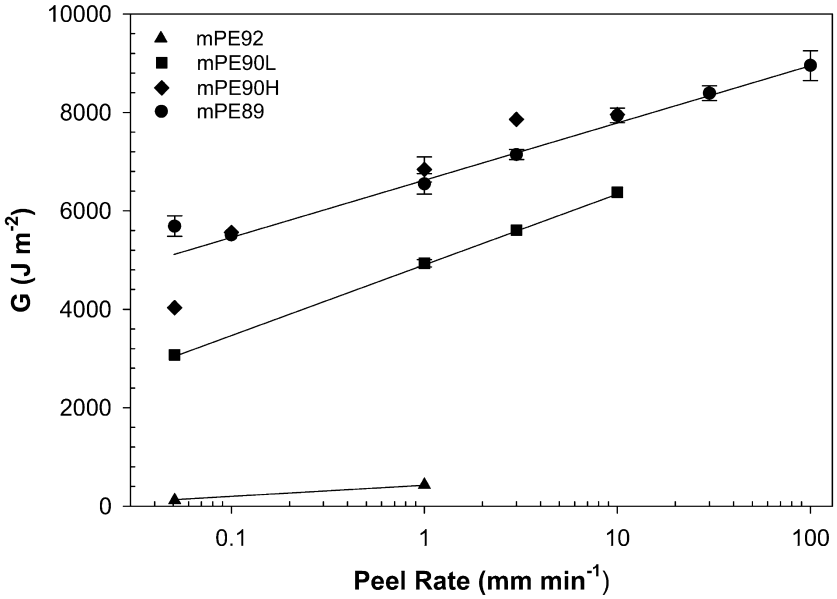

Fig. 3. Effect of peel rate on measured delamination toughness.

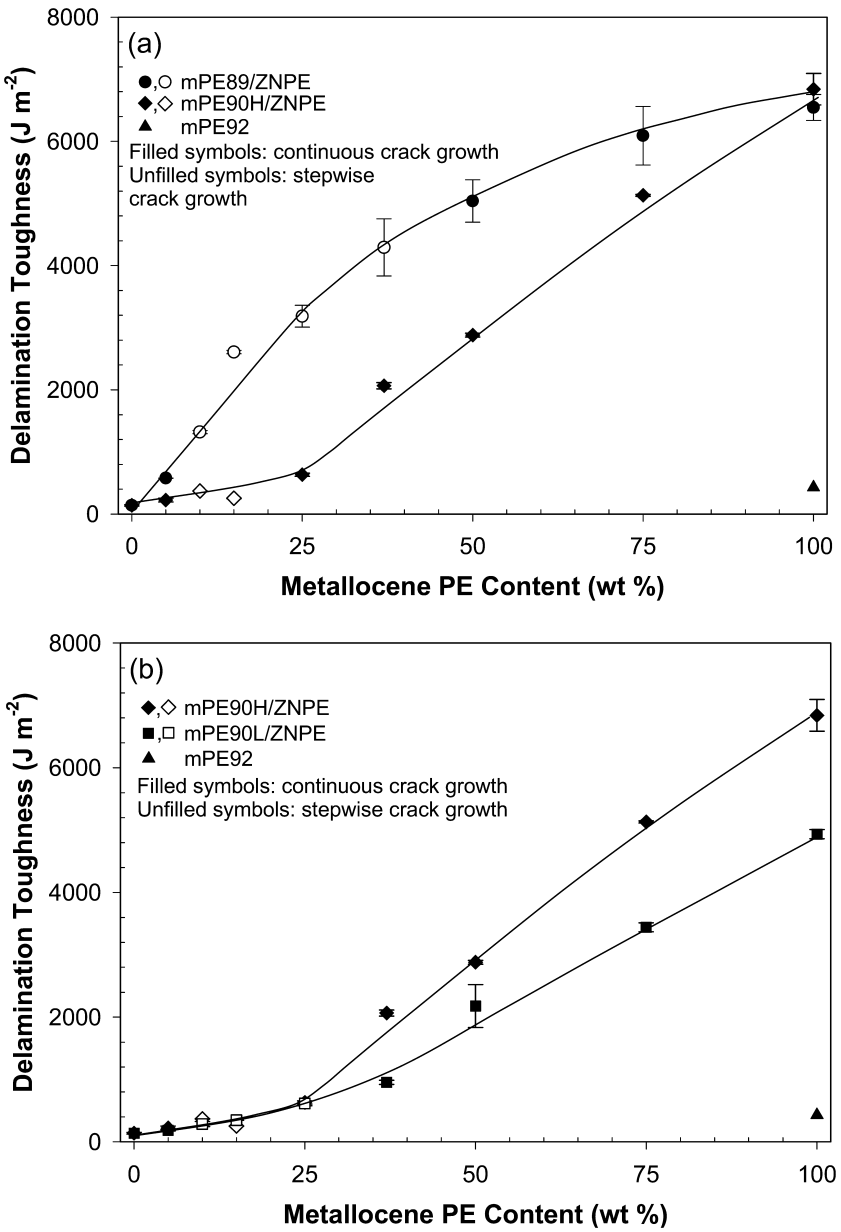

Fig. 4. Effect of blend composition on delamination toughness measured at a peel rate of 1 mm min^{-1}: (a) effect of SCB content; and (b) effect of molecular weight.

density polyethylenes produced by conventional Ziegler-Natta catalysts are characterized by a wide molecular weight distribution and considerable nonuniformity in comonomer distribution. Chains with highest concentration of short chain branches are also those in the low molecular weight tail of the molecular weight distribution. Short chains that are driven to the interface by entropic contributions to the chemical potential also have an enthalpic advantage due to the high branch content. The molecular weight of these amorphous chains is too low to provide entanglements required for good adhesion.

In order to expose the surface of the polyethylene layer for examination, ZNPE and ZNPE blends were microlayered with PS. The polyethylene layers experienced the same process history as in microlayers with PP. The same thermodynamic forces that drove low molecular weight fractions to the interface with PP also drove them to the PS interface. Polyethylene layers separated easily from PS layers without damaging the surfaces. In AFM phase images, soft amorphous material appeared dark and hard crystalline material appeared bright. Fig. 5a shows the exposed ZNPE surface with a coating of soft material filling the spaces between occasional bright segments of lamellar crystals. With normal tapping conditions, the AFM tip did not completely penetrate the soft coating to entirely reveal the crystalline morphology. Harder tapping conditions were required for the tip to completely penetrate the soft coating and expose the underlying lamellar spherulites.

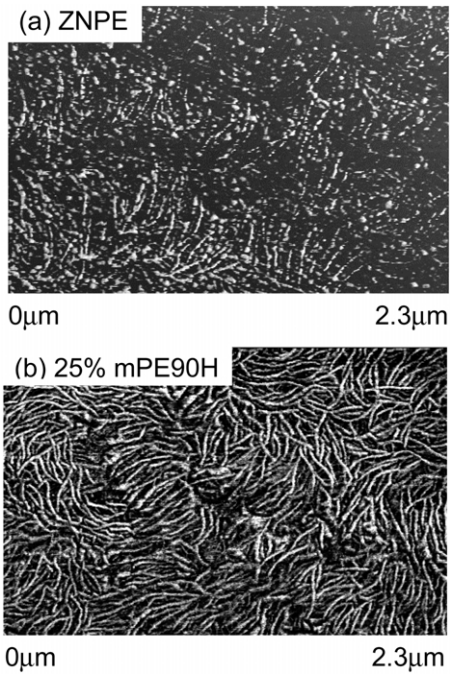

Fig. 5. AFM phase images of unwashed microlayer surfaces: (a) ZNPE; and (b) ZNPE blended with 25% mPE90H.

The thickness of the coating, as estimated from the penetration depth of the AFM tip using the force-probe method, was approximately 8 nm [9].

Blending ZNPE with mPE of higher branch content resolved the amorphous interfacial layer by enhancing miscibility of highly branched ZNPE fractions in the bulk. The exposed surface of a ZNPE blend with 25% mPE90H in Fig. 5b, imaged with the same tapping conditions used in Fig. 5a, shows that the amorphous surface coating was absent from the blend. Normal tapping conditions fully revealed the lamellar morphology in a segment of banded spherulite. Resolution of the amorphous interfacial layer that impeded intimate contact of bulk ZNPE chains with PP increased G by about a factor of 3 (Fig. 4). Whereas resolution of the amorphous interfacial layer required blending with 25% of mPE90H, only 5% of mPE89 with higher SCB content had the same effect. Considerable overlap in SCB distribution (Fig. 1) between the main fractions of mPE89 and the highly branched tail of ZNPE maximized miscibility of highly branched ZNPE fractions in the bulk. The main fractions of mPE90H and mPE90L did not overlap with the highly branched ZNPE fractions as well as the main fractions of mPE89 did in terms of SCB distribution. Consequently, more mPE90H or mPE90L was required to prevent highly branched ZNPE fractions from segregating at the interface.

3.3. Phase separation

The very substantial increase in G as the blend was enriched with mPE beyond the amount required to resolve the amorphous interfacial layer needed another explanation. To identify other factors affecting G, the phase morphology of ZNPE blends with mPE was examined. All the mPEs were miscible with ZNPE in the melt according to studies that establish the difference in comonomer content for melt miscibility at $\sim$8 mol% for this molecular weight range [13]. Melt miscibility was confirmed by observation of a single texture in AFM images of ZNPE blends with 25% mPE89 or 25% mPE90H that had been quenched into a dry ice/ethanol bath from 230 °C according to procedures established previously [13]. However, cooling in the microlayer process was slow enough for crystallization to produce phase separation.

Phase separation in microlayers was examined by comparing exposed surfaces of ZNPE, mPE90H, and a blend with 25% mPE90H. Before imaging ZNPE, the surface was washed with ethanol to remove the amorphous coating. The underlying crystalline morphology consisted

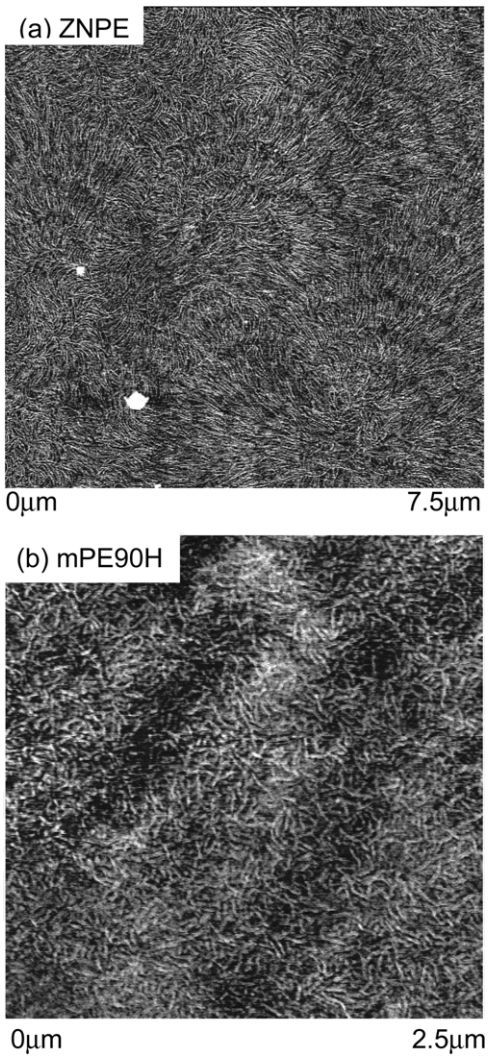

Fig. 6. AFM phase images: (a) surface of ZNPE after washing with ethanol; and (b) surface of unwashed mPE90H.

of space-filling spherulites, Fig. 6a. Because mPE90H did not contain fractions with SCB content different from the bulk, an amorphous interfacial layer did not exist and the exposed surface did not need to be washed in order to image the crystalline morphology. The unwashed mPE90H surface consisted of unorganized lamellae of thickness 20 nm and length 200–300 nm, Fig. 6b, which are characteristic of mPE with this SCB content if it is rapidly cooled from the melt [14].

On the unwashed surface of ZNPE blended with 25% mPE90H, large banded spherulites were separated by interspherulitic regions of unorganized, short wavy lamellae, Fig. 7a. A higher resolution image of the spherulite boundary, Fig. 7b, revealed two textures and confirmed phase separation during crystallization. It appeared that ZNPE bulk chains crystallized as spherulites during cooling and rejected mPE90H together with low molecular weight, highly branched fractions of ZNPE into the interspherulitic regions. The ZNPE spherulites had diameter of 7 μm and lamellae had thickness of 20 nm. They closely resembled the space-filling spherulites of the ZNPE surface (Fig. 6a) except that the banding period was smaller, 450 nm compared to 500 nm. The smaller banding period in the blend probably resulted from a lower crystallization temperature [15]. The texture of the interspherulitic regions closely resembled the texture of mPE90H (Fig. 6b) with unorganized lamellae of thickness 20 nm and length 200–300 nm. The lamellae appeared somewhat more defective in the blend, probably due to the presence of low molecular weight, amorphous ZNPE fractions. The two-phase nature of the blend could account for the compositional dependence of G if the mPE phase adhered better to PP than did the ZNPE phase.

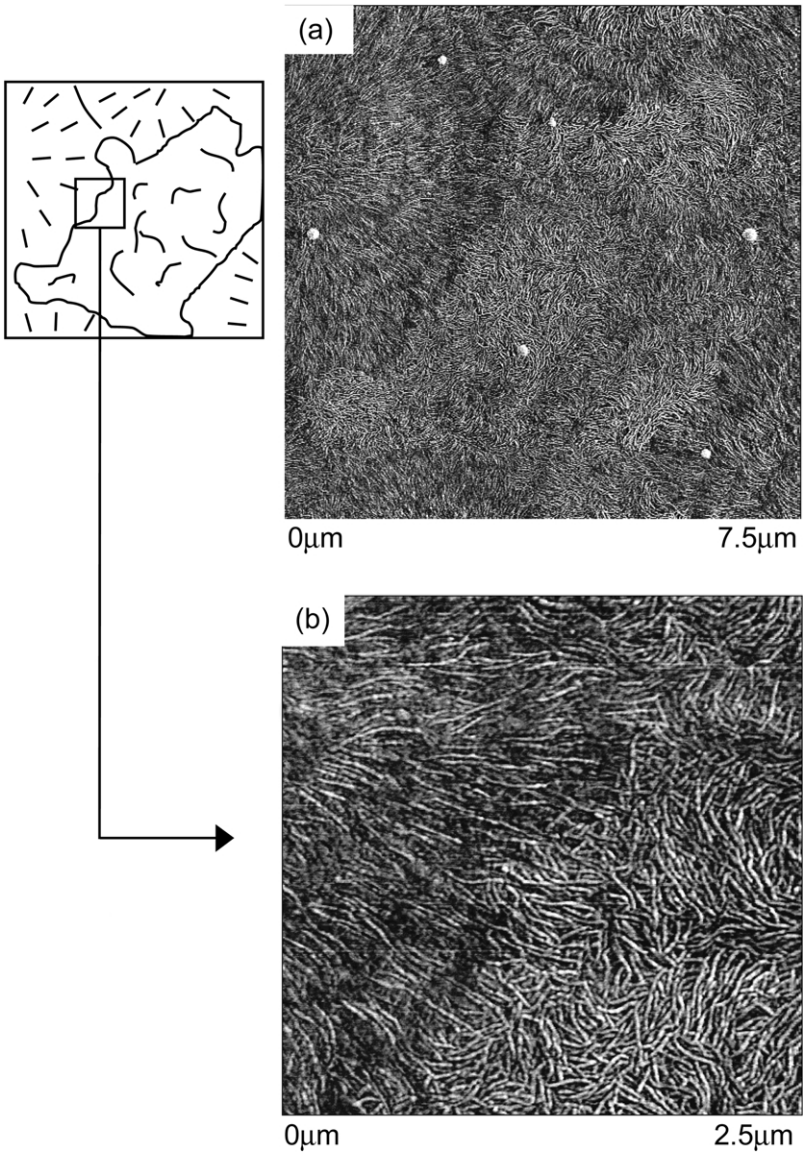

Fig. 7. AFM phase image of the unwashed surface of ZNPE blended with 25% mPE90H: (a) lower magnification showing phase separation; and (b) higher magnification showing phase textures.

3.4. Layer interface

The interface between an ethylene copolymer layer and a PP layer in microlayers was imaged in cross-section by AFM. The interface in Fig. 8a between ZNPE (upper layer) and PP (lower layer) was sharp and straight. The PP layer crystallized first as the microlayer was cooled from the melt. Although the ~8 nm amorphous interfacial layer was too thin to be visible in AFM images, it effectively prevented epitaxial crystallization of ZNPE on PP. The ZNPE layer showed part of a spherulite that had nucleated within the layer and had grown toward the interface until it impinged on the crystallized PP layer.

The blend with 25% mPE90H had a thin layer about 200 nm thick of organized PE lamellae at the interface, Fig. 8b. Epitaxial crystallization of polyethylene on polypropylene is well-known [16,17], and has been observed in their melt blends [18]. The small lamellae were mostly aligned parallel to the interface although sometimes they were arranged at the characteristic angle of about 40°. The aligned lamellae separated the PP layer at the bottom of the image from the edge of a PE spherulite at the top of the image. The spherulite nucleated within the layer and grew toward the epitaxial layer. Blending ZNPE with 25% mPE90H was sufficient to resolve the amorphous interfacial layer and expose bulk ZNPE chains to the interface, where they epitaxially crystallized during cooling. Epitaxial crystallization increased G from 140 J m^{-2} for ZNPE to 630 J m^{-2} for the blend with 25% mPE90H. Epitaxial crystallization of homogeneous mPE with about the same SCB content as ZNPE bulk chains produced a comparable G of 430 J m^{-2} [9].

A cross-section of the blend with 50% mPE90H also showed an aligned layer of epitaxially crystallized lamellae that extended about 200 nm from the interface, Fig. 8c. In addition to the aligned lamellae, there were regions, where the interface was indistinct and it was difficult to distinguish a boundary between PP and PE lamellae (arrow). These appeared to be regions where the mPE90H phase contacted the PP layer. Possibly interdiffusion and entanglement of chains in the mPE90H phase produced better adhesion to PP than epitaxial crystallization of bulk chains in the ZNPE phase. The blend with 50% mPE90H had considerably higher G than the blend with 25% mPE90H, 2900 J m^{-2} compared to 630 J m^{-2}.

The diffuse, poorly defined interface, Fig. 8d, and high

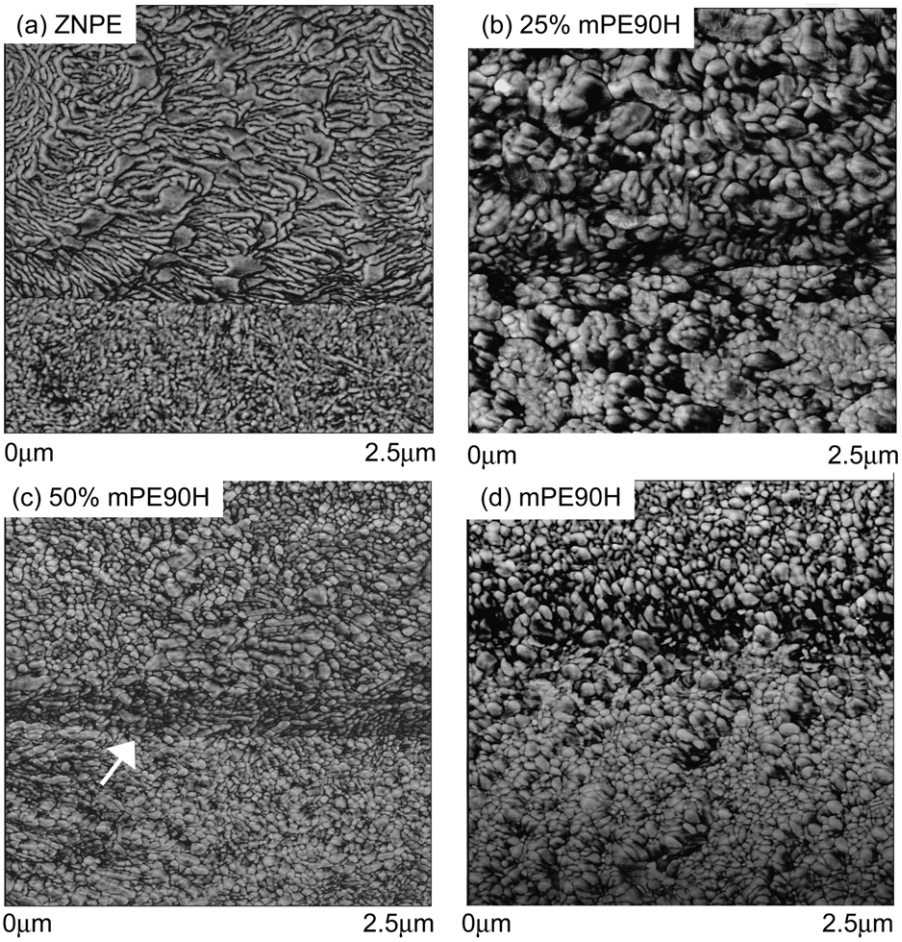

Fig. 8. AFM phase images of microlayer cross-sections showing the interface between an ethylene copolymer (upper layer) and PP (lower layer): (a) ZNPE; (b) ZNPE blended with 25% mPE90H; (c) ZNPE blended with 50% mPE90H; and (d) mPE90H.

delamination toughness, 6800 J m^{-2}, of mPE90H were consistent with interdiffusion and entanglement of mPE90H chains. The granular crystalline texture of mPE90H in this image was probably due to uneven etching of this low crystallinity material. However, the absence of a layer of aligned lamellae at the mPE90H interface confirmed that bulk chains of ZNPE comprised the epitaxially crystallized lamellae of the blends (Fig. 8b and c).

3.5. Interfacial model

Interaction of an ethylene copolymer with PP begins at the melt interface during coextrusion. Although polyethylene and polypropylene are generally considered to be immiscible, some amount of chain interdiffusion and entanglement at the melt interface is expected. The interpenetration depth d can be estimated according to Ref. [19]

$$d = \frac{2b}{\sqrt{6\chi_{PP-PE}}} \quad (1)$$

where the characteristic bond length b is approximately 7 Å and χ_{PP-PE} is the interaction parameter. To estimate χ_{PP-PE}, reported values of the solubility parameter δ for copolymers of different SCB content [20] were used to obtain χ_{PP-PE} at two temperatures according to Ref. [21]

$$\chi_{PP-PE} = \frac{V}{RT}(\delta_{PP} - \delta_{PE})^2 \quad (2)$$

where the molar volume V was taken as 32.8 cm^3 mol^{-1}. Subsequently, χ_{PP-PE} at 230 °C was estimated from the reported temperature dependence of χ [13]

$$\chi = a + \frac{b}{T} \quad (3)$$

Calculated interpenetration depths ranged from 60 Å for mPE89 to 40 Å for mPE92 and bulk chains of ZNPE. A depth of 50 Å corresponded to approximately twice the radius of gyration of the entanglement molecular weight (M_e) of PP and three times that of PE [22,23], which was more than the minimum effective segment length of one M_e [24].

The role of entanglements is considered in the proposed structural model for adhesion to PP in microlayers as presented in Fig. 9. Beginning with ZNPE, the low molecular weight, highly branched fractions segregate to the PP interface due to entropic and enthalpic forces. Although these chains can interdiffuse with PP, their molecular weight is too low to produce effective entanglements. Furthermore, there is no advantage for bulk chains to diffuse through the amorphous layer to form entanglements. After solidification, the amorphous interfacial layer does not impart good adhesion to PP. In contrast to ZNPE, homogeneous copolymers do not possess low molecular weight fractions with composition different from the bulk and the melt interface is readily accessible to interdiffusion of bulk chains.

However, even if bulk chains are available at the melt interface to interdiffuse, the result may not be good adhesion, as illustrated by relatively low G of mPE92 compared to mPE90L, mPE90H, and mPE89. The dependence of interpenetration depth on SCB content estimated from Eq. (1) is not large enough to account for the order of magnitude variation in G. This suggests that the extent to which entanglement bridges, formed in the melt, remain effective after solidification depends on SCB content.

Entanglement loss during crystallization is thought to be the reason that slowly cooled laminates of high density polyethylene and PP exhibit lower adhesion than rapidly cooled laminates [25]. Similarly, it is suggested that entanglement bridges, formed by interdiffusion in the microlayer melt, can be lost as a result of crystallization during cooling. As the melt cools, crystallization of PP provides the driving force for disentanglement of PP chains from the ethylene copolymer melt. Copolymer chains can remain entangled in the noncrystalline regions of PP, however, subsequent disentanglement is possible when the copolymer crystallizes at a lower temperature. It is proposed that the relatively low G value of mPE92 results from loss of entanglement bridges driven by epitaxial crystallization at the PP interface, Fig. 9. The same concept applies to ZNPE after the amorphous layer is resolved by blending with mPE. Epitaxial crystallization of ZNPE bulk chains imparts some level of adhesion to PP [26,27], however, the level of adhesion that entangled chains would have provided is not achieved.

Compared to mPE92 and ZNPE bulk chains, crystallization is less of a driving force for disentanglement of mPE89, mPE90L and mPE90H. With fewer and shorter crystallizable chain segments, crystallization provides less of an energetic incentive for disentanglement. Excellent adhesion to PP, as indicated by very high G values, is attributed to persistence of entanglement bridges after the copolymer is fully crystallized, Fig. 9. The markedly higher G of mPE90H compared to mPE90L is consistent with the larger number of entanglement bridges formed by a polymer molecule of higher molecular weight.

In blends of ZNPE with mPE, increasing the mPE content past the amount required to completely resolve the amorphous interfacial layer of ZNPE results in a steady, almost linear, increase in G. It can be imagined that phase separation during crystallization of ZNPE bulk chains produces a mixed interface with regions of epitaxial crystallization, where the ZNPE phase contacts the interface, and other regions with entanglement bridges, where the mPE phase contacts the interface, Fig. 9. Because entanglement bridges impart much stronger adhesion than do epitaxially crystallized lamellae, G increases with the amount of the mPE phase. The relationship is surprisingly linear.

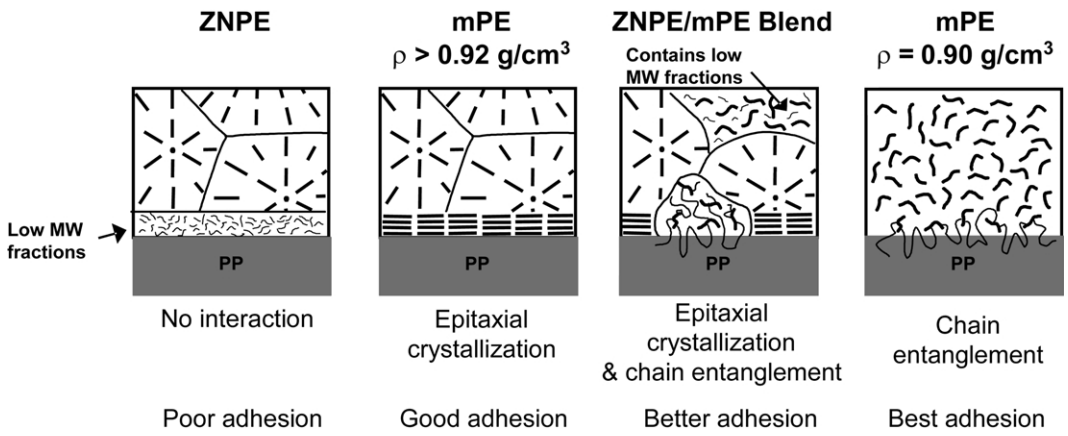

Fig. 9. Model for the interface of PP with ZNPE, mPE, and their blends.

4. Conclusions

Ethylene copolymers available today present a wide range of chain microstructures in terms of SCB content, branch distribution, molecular weight, and molecular weight distribution. Combining copolymers as blends further extends the rich variety of available microstructural compositions. Utilizing appropriate structure–property relationships, it is possible to tailor microstructural composition to achieve specific attributes. In this study, we were interested in the relationship between chain microstructure and adhesion to PP. Coextruded microlayers provided convenient access to the interface between PP and an ethylene copolymer or copolymer blend for both adhesion and structural characterization.

It was possible to vary adhesion of an ethylene copolymer to PP by more than an order of magnitude as measured by delamination toughness. The best adhesion was achieved with higher molecular weight mPE having density of 0.90 g cm^{-3} or less. Good adhesion of low crystallinity ethylene copolymers was attributed to entanglement bridges that were created in the melt and persisted during solidification. Poorer adhesion of a homogeneous copolymer of density 0.92 g cm^{-3} was attributed to loss of entanglement bridges driven by epitaxial crystallization of the higher crystallinity copolymer. Very poor adhesion of heterogeneous ZNPE was attributed to an amorphous interfacial layer of highly branched chains having molecular weight too low to form effective entanglement bridges. The interfacial layer could be resolved by blending ZNPE with mPE of lower density. However, adhesion increased only modestly because the bulk chains of ZNPE disentangled when they crystallized epitaxially on PP. Intermediate adhesion to PP was achieved by blending ZNPE with mPE beyond the amount required to resolve the amorphous interfacial layer.

Acknowledgements

The technical assistance of Dr L. Tau of The Dow Chemical Company is gratefully acknowledged. Financial support for this research was provided by The Dow Chemical Company.

References

[1] Utracki LA, Dumoulin MM. Polypropylene alloys and blends with thermoplastics. In: Karger-Kocsis J, editor. Polypropylene structure, blends, and composites. Copolymers and blends, vol. 2. New York: Chapman and Hall; 1995. p. 50.
[2] Ewen JA. Metallocene polymerization catalysts: past, present and future. In: Scheirs J, Kaminsky W, editors. Metallocene-based polyolefins, vol. 1. New York: Wiley; 2000. p. 3.
[3] Soga K, Uozumi T, Kaji E. Synthesis of isotactic polypropylene by metallocene and related catalysts. In: Scheirs J, Kaminsky W, editors. Metallocene-based polyolefins, vol. 1. New York: Wiley; 2000. p. 381.
[4] Arnold M, Bornemann S, Köller F, Menke TJ, Kressler J. Macromol Chem Phys 1998;199:2647–53.
[5] Mueller CD, Nazarenko S, Ebeling T, Schuman T, Hiltner A, Baer E. Polym Engng Sci 1997;37:355–62.
[6] Mueller C, Topolkaraev V, Soerens D, Hiltner A, Baer E. J Appl Polym Sci 2000;78:816–28.
[7] Ebeling T, Hiltner A, Baer E. J Appl Polym Sci 1998;68:793–805.
[8] Späth T, Plogmaker D, Keiter S, Petermann J. J Mater Sci 1998;33:5739–45.
[9] Poon BC, Chum SP, Hiltner A, Baer E. J Appl Polym Sci 2003; in press.
[10] Olley RH, Bassett DC. Polymer 1982;23:1707–10.
[11] Kinloch AJ. Adhesion and adhesives: science and technology. London: Chapman and Hall; 1987. p. 300–38.
[12] Ebeling T, Hiltner A, Baer E. Polymer 1999;40:1525–36.
[13] Stephens CH, Hiltner A, Baer E. Macromolecules 2003;36:2733–41.
[14] Bensason S, Minick J, Moet A, Chum S, Hiltner A, Baer E. J Polym Sci Part B: Polym Phys 1996;34:1301–15.
[15] Keith HD, Padden FJ. Macromolecules 1996;29:7776–86.
[16] Lotz B, Wittman JC. J Polym Sci Part B: Polym Phys 1987;25:1079–87.
[17] Wittman JC, Lotz B. Prog Polym Sci 1990;15:909–48.
[18] Chang AC, Chum SP, Hiltner A, Baer E. Polymer 2002;43:4923–33.
[19] Helfand E, Tagami Y. J Chem Phys 1972;56:3592–601.
[20] Han SJ, Lohse DJ, Condo PD, Sperling LH. J Polym Sci Part B: Polym Phys 1999;37:2835–44.
[21] Wool RP. Polymer interfaces. Munich: Hanser; 1995. p. 383.

[22] Chafin KA, Bates FS, Brant P, Brown GM. J Polym Sci Part B: Polym Phys 2000;38:108–21.
[23] Fetters LJ, Lohse DJ, Richter D, Witten TA, Zirkel A. Macromolecules 1994;27:4639–47.
[24] Creton C, Kramer EJ, Hadziiannou G. Macromolecules 1991;24:1846–53.
[25] Shibayama M, Izutani A, Ishikawa A, Tanaka K, Nomura S. Polymer 1994;35:271–80.
[26] Chang AC, Chum SP, Hiltner A, Baer E. Polymer 2002;43:6515–26.
[27] Kestenbach H-J, Loos J, Petermann J. Polym Engng Sci 1998;38:478–84.